Chapter 2

# Advances in Design and Self-Assembly of Functionalized LB Films and Supramolecular Gels

Tifeng Jiao, Ruirui Xing, Kai Ma and Lexin Zhang

Additional information is available at the end of the chapter

http://dx.doi.org/10.5772/65122

**Abstract**

The recent progress in functionalized LB films and supramolecular gels varies and occupies various fields. Self-assembly technique is playing an important role in preparing well-defined multilevel nanostructures and the functionalized nanomaterials with the designed and controlled properties. In this chapter, various kinds of functionalized LB films and supramolecular gels, including gold nanoparticles, inorganic-organic hybrid composites, and graphene oxide nanocomposites, have been demonstrated and analyzed. We show main research contributions in recent years in two sections: preparation and self-assembly of some functionalized LB films and preparation and self-assembly of some functionalized supramolecular gels. The above research work may give the potential perspective for the design and preparation of new self-assembly nanomaterials. Future research on preparation of LB films and supramolecular gels will depend on the novel applications and special nanostructures in order to produce novel functional nanomaterials and devices.

**Keywords:** LB film, supramolecular gel, self-assembly, nanomaterials, nanostructures, properties

## 1. Introduction

The recent progress in functionalized LB films and supramolecular gels is varied and occupies various fields. It is well known that the self-assembly techniques demonstrate important and crucial role to prepare various functionalized nanostructures and nanomaterials with the preferred properties. In comparison with the conventional self-assembly process of amphiphiles in bulk or at interfaces, the self-assembly process of inorganic-organic hybrids,

nanoparticles and colloidal microspheres, and supramolecular nanostructures show special properties, especially in preparing complicated nanocomposites or nanomaterials.

In the recent reports in our groups, some systems, including LB films and supramolecular gels, have been designed and characterized. In addition, some useful analytical techniques and synthetic treatments applied in supramolecular self-assembly field have been highlighted and analyzed. In the present chapter, we summarize main work contributions in recent years in two parts: (1) preparation and self-assembly of some functionalized LB films and (2) preparation and self-assembly of some functionalized supramolecular gels.

## 2. Preparation and self-assembly of some functionalized LB films

The Langmuir-Blodgett technique is an important method to produce macroscopic materials organized on the molecular scale [1–5]. This approach allows amphiphilic molecules to be oriented at the air-water interface and then transferred sequentially onto a solid support [6–15]. In our research, some special amphiphiles, including bolaamphiphiles, gemini, and amphiphiles with functional substituted groups, have been designed and synthesized, and their organized supramolecular assemblies in LB films have also been investigated, which may broaden the traditional research areas about LB film and give some perspectives and clues for the relative research in the future.

Firstly, in our previous work, a bolaform and single chain Schiff base, abbreviated as BSC10 and HBOA, have been synthesized and their interfacial self-assembly in LB films and interaction with barbituric acid (BA) was demonstrated [16]. It has been found that while HBOA formed a monolayer at the air/water interface, the bolaform Schiff base formed a multilayer film with ordered layer structure on water surface. The relative interfacial morphologies were shown in **Figure 1**. The detailed investigations of the transferred multilayer films were characterized by various spectral techniques. A clear conformational change of the alkyl spacer in the bolaform Schiff base was observed during the complex formation with the barbituric acid. In the obtained self-assembly unit, the alkyl spacer showed obvious bent/gauche conformation due to the H-bond requirement. So, direct experimental data about conformation change of alkyl chains in LB films were clearly demonstrated.

In addition, the interfacial films of a series of designed gemini amphiphiles containing the Schiff base moiety have been investigated [17]. This series of gemini amphiphiles with Schiff base headgroups linked by a hydrophobic alkyl spacer (BisSBC18Cn, n = 2, 4, 6, 8, 10) could be spread to form stable monolayers and coordinated with Cu(II) ions in the monolayer. The Langmuir films of gemini amphiphiles with the spacer length of six or eight methylene groups demonstrated maximum limiting molecular area. Nanonail and tape-like morphologies were observed for amphiphile films with shorter spacers (n = 2 and 4) on the water surface. Worm-like morphologies were observed for gemini films with longer spacers of C8 and C10 when coordinated with Cu(II) ions, as illustrated in **Figure 2**. For the compounds with short spacer, the spacer showed parallel organization to the water surface. With length increment, the spacer

http://dx.doi.org/10.5772/65122

part could show bent/gauche conformation. Therefore, the films with spacer lengths of C6 and C8 on water and Cu(II) ions demonstrated maximum limiting molecular areas, respectively.

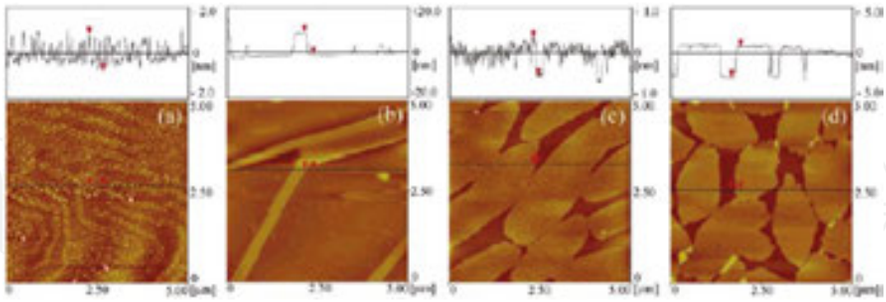

**Figure 1.** AFM images of monolayer LB films of bolaform Schiff base (HBOA) from pure water subphase and 1.0 mM BA subphase.

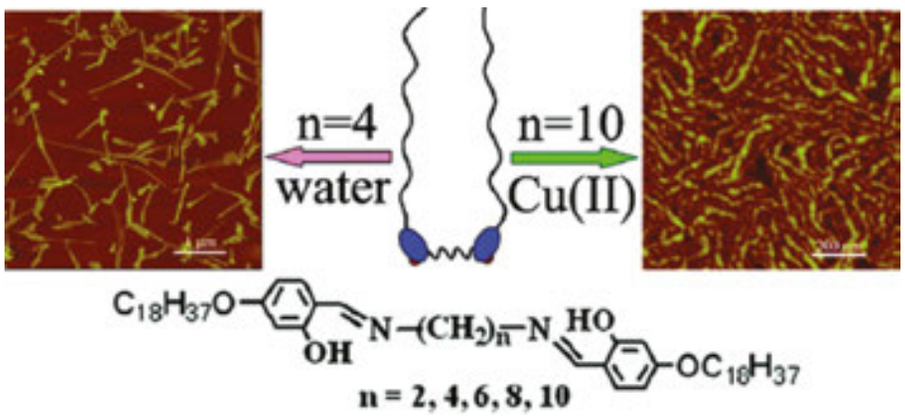


**Figure 2.** Schematic illustration of the packing modes of BisSBC18Cn in organized films.

In another research work, a tyrosine-based bolaamphiphile (abbreviated as C10BT) has been designed and its interfacial assemblies were investigated [18]. It was interesting to find that metal ions, such as Ag(I) and Cu(II) ions, in the subphase can greatly modulate the molecular packing of C10BT and the morphology of the subsequently deposited LB films. The X-ray diffraction and X-ray photoelectron spectra verified the orderly layer structure and the relative molar ratios compared with different metal ions. Quantitative analysis of XPS data indicated the values of 1:1.95 for C10BT:Ag(I) and 1:1.08 for C10BT:Cu(II). Considering the coordination process and spectral results, as shown in **Figure 3**, a rational self-assembly process has been proposed. For the Cu(II)-coordinated film, the molecules were connected by coordination sites with spacer in bent conformation. On the other hand, for Ag(I)-complexed film, the molecules were orderly stacked by cooperative forces.

Next, we have also investigated the interfacial self-assembly of a block-type polymer abbreviated as $PEO_{45}$-b-$PDMA_{69}$ by the LB technique [19]. Accompanied by a pancake-to-brush transition of PEO conformation, the worm-like surface micelles are compression induced, as shown in **Figure 4**. The micelles as the building blocks can be arrayed parallel to generate a

long-range ordered structure, further bended and twisted upon compression. The obtained nanostructure change could be assigned to the special coil-semirod molecular structures and the unique capability of the PDMA part. The research work gives exploration for preparing functional polymers and nanostructures in organized films.

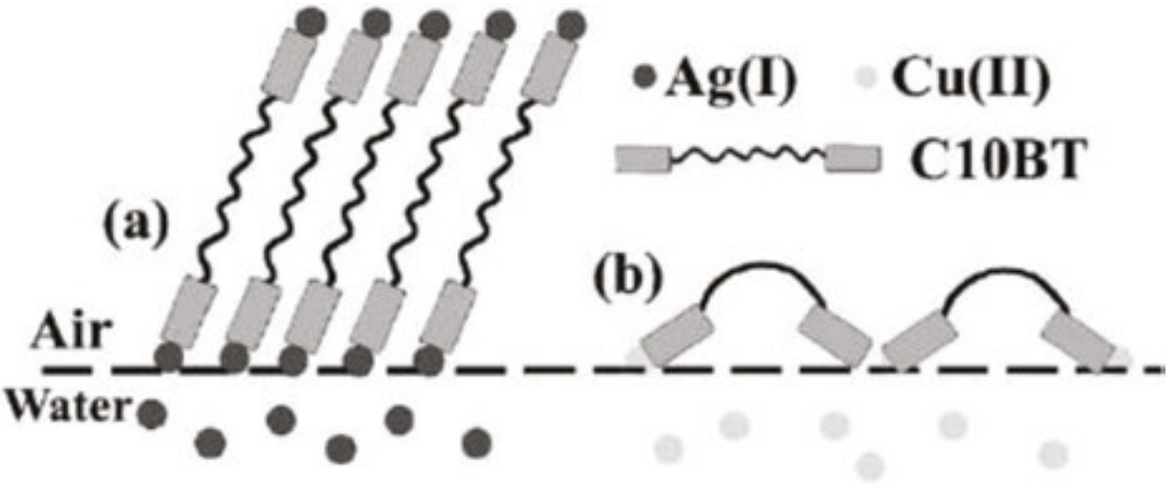


**Figure 3.** Cartoon illustration of the packing modes for C10BT complex films on different subphases: (a) Ag(I) ions subphase; (b) Cu(II) ions subphase.

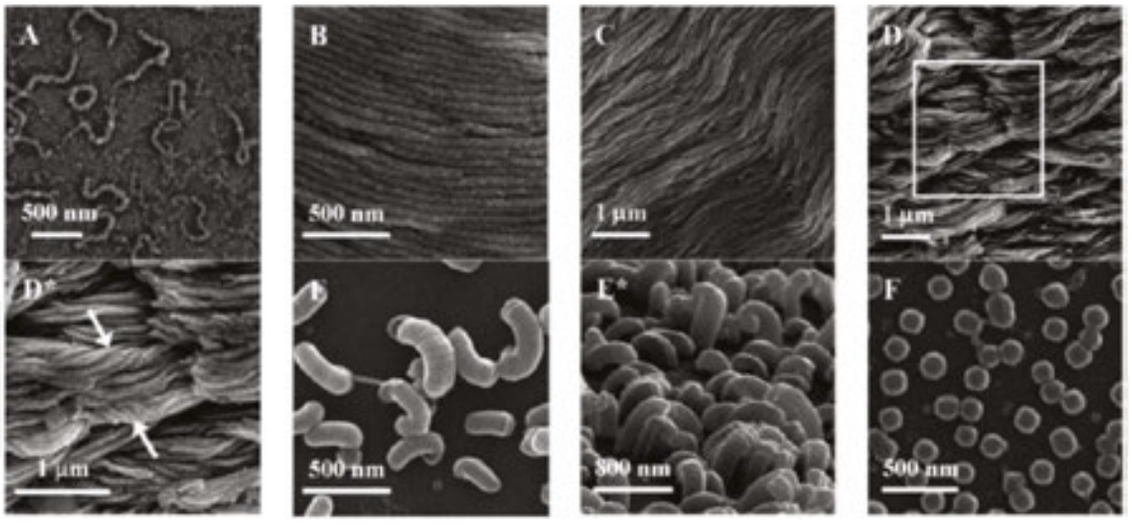


**Figure 4.** SEM images of the LB films at various molecular areas: (A) 28 $nm^2$/molecule; (B) 21 $nm^2$/molecule; (C) 16 $nm^2$/molecule; (D) 13 $nm^2$/molecule; (E) 7 $nm^2$/molecule; (F) 5 $nm^2$/molecule.

In another work, two coumarin derivatives were synthesized and their interfacial self-assemblies were investigated [20]. Owing to the different substituent position of the long octadecyloxy chain in the coumarin parent, the two compounds showed obviously different interfacial behaviors. The spreading films on the water surface were transferred onto solid substrates and characterized by various spectra and atomic force microscopy (AFM). Different

http://dx.doi.org/10.5772/65122

packing of the molecules in the multilayer films was observed, as shown in **Figure 5**. Photoreaction could not occur in 4-CUMC18 film due to possible large steric hindrance, while photochemical reaction produced in 7-CUMC18 film because of the face-to-face stacking of benzene ring and steric matching.

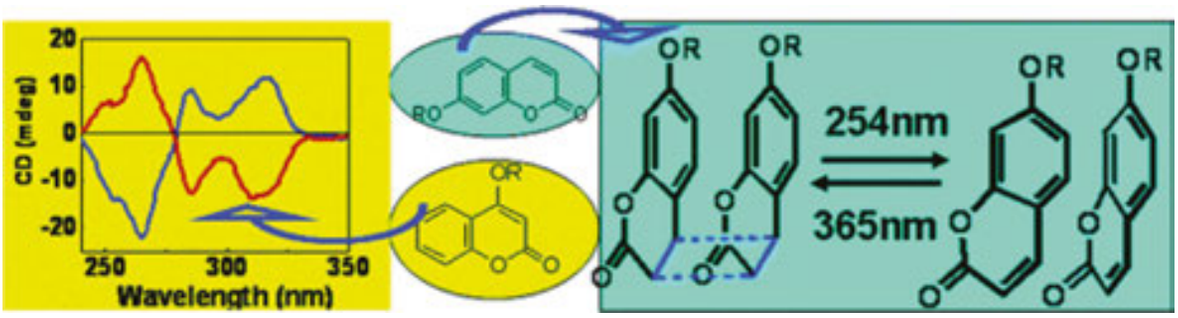


**Figure 5.** Illustration of the possible packing and photoreaction in the LS films.

In addition, preparation and characterization of gemini amphiphiles-gold nanostructure composite films have been demonstrated [21]. The as-formed composite monolayer films with gold nanoparticles generated by chemical or photochemical reduction in film were transferred, as shown in **Figure 6**. When UV illumination was used, gold nanoparticles can be produced. Upon subsequent reduction process in solution, the preformed nanoparticles could grow into different nanostructures as seeds and further self-assemble into larger structures in solution. This research work provided a simple way to control the aggregates and optical properties of gold nanostructures by adjusting the initial irradiation time.

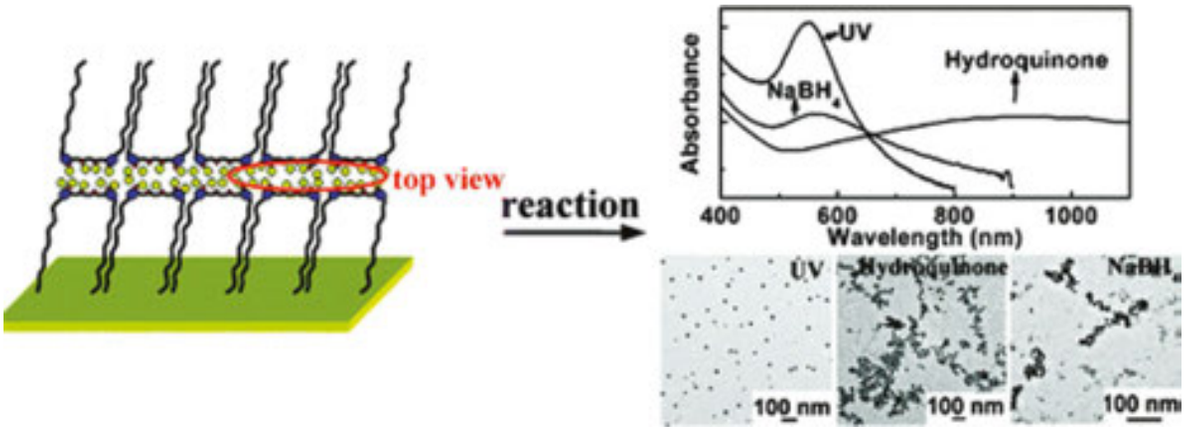


**Figure 6.** Schematic illustration on the generation of gold nanoparticles by photochemical and chemical reduction in GN2/$AuCl_4^-$ complex film.

In another research work, two luminol derivatives with different substituted chains (abbreviated as LC11 and TF46) were mixed with glycolipid compound GC11 to form monolayers at the air-water interface [22]. The pure and mixed interfacial Langmuir films were studied by measuring the surface pressure-molecular area isotherms, and their morphologies were

characterized by Brewster angle microscopy (BAM), as shown in **Figure 7**. Dot-like domains were observed by BAM for TF46 Langmuir films, contrariwise to some strip-like aggregated domains in the case of LC11. These different morphologies may be attributed to distinct aggregation modes induced by differences in molecular structure.

In addition, in order to insert the noninhibitory anti-choline oxidase immunoglobulin (anti-ChOD IgG), mixed IgG-TF46 vesicles have been prepared and spread on a phosphate buffered saline (PBS) subphase [23]. The formation of the interfacial film, after disruption of the IgG-TF46 vesicle membranes at the air-liquid interface, has been evidenced by liposome fusion process and LB method. When acting as an electrochemiluminescent (ECL) sensor, the designed self-assembly films demonstrated capability of biomimetic sensor, as shown in **Figure 8**. The relative research work showed the exploration of application of luminol derivatives to form functional films for ECL detection.

In addition, some Schiff base compounds with trigonal molecular skeletons were prepared and the interfacial self-assembly process were characterized [24]. The Cu(II)-coordinated films could be transferred and characterized by various spectral and morphological methods. As shown in **Figure 9**, depending on different substituted headgroups and subphase solutions, various morphologies were obtained. Moreover, on different pH subphases, the interfacial assembly and nanostructures varied obviously. And reasonable explanation about the self-assembly behaviors have been proposed.

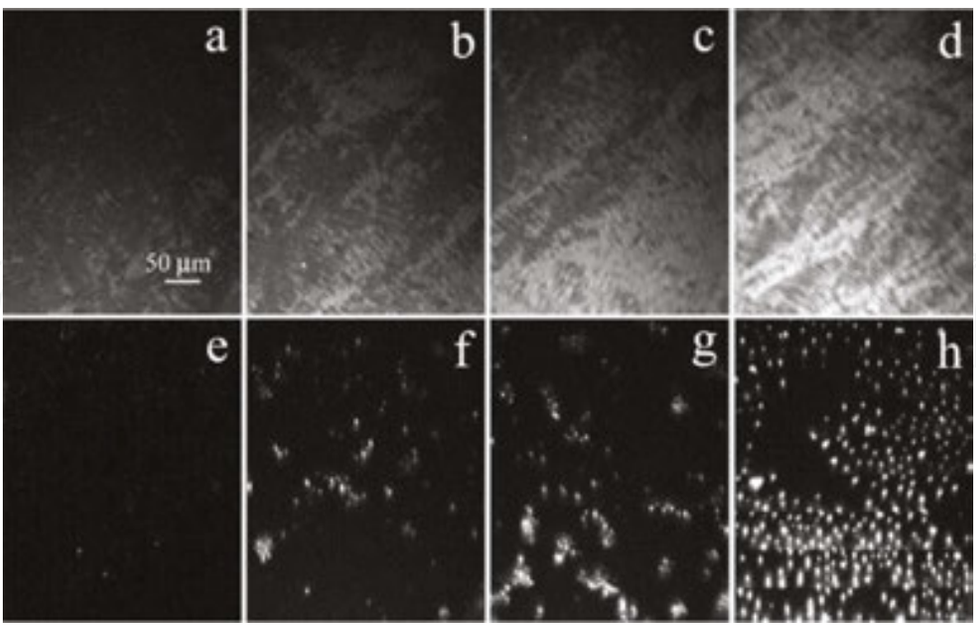


**Figure 7.** BAM images of LC11 and mixed LC11/GC11 monolayers at different surface pressures. For LC11 monolayer: (a) 5 mN/m; (b) 18 mN/m; (c) 24 mN/m; (d) 36 mN/m. For mixed LC11/GC11 monolayer: (e) 23 mN/m; (f) 28 mN/m; (g) 29 mN/m; (h) 31 mN/m.

http://dx.doi.org/10.5772/65122

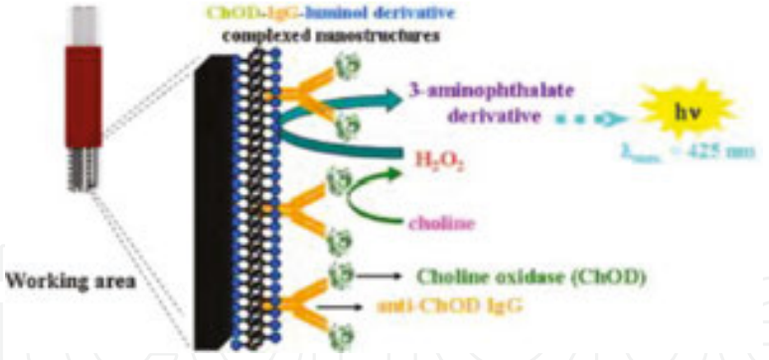


**Figure 8.** Reagentless detection principle of choline oxidase activity by ECL reaction triggered directly in the sensing layer.

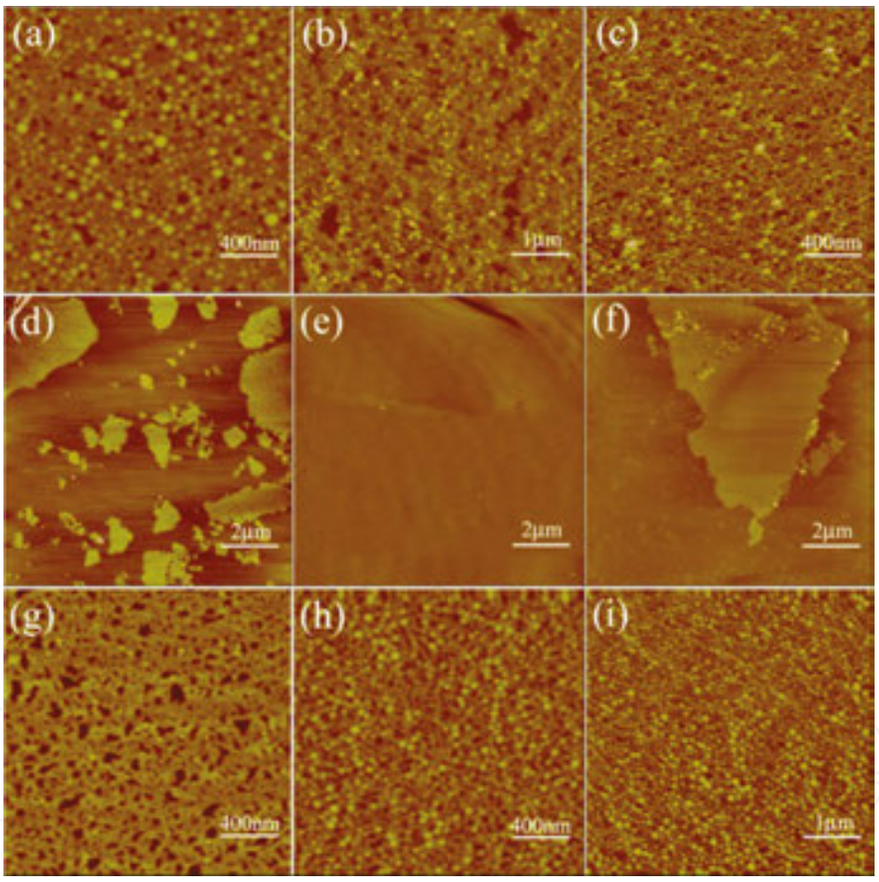


**Figure 9.** AFM images of one layer TSB-Sal, TSB-Np and TSB-C16 films deposited from pure water surface (a, d, g), aqueous 1.0 mM $Cu(Ac)_2$ subphase (b, e, h), and aqueous 1.0 mM $Zn(Ac)_2$ subphase (c, f, i) at 15 mN/m, respectively.

In addition, we have reported the design and preparation of LB films of an aromatic Schiff base compound and relative Cu(II)-complex [25]. We found that the synthesized compound abbreviated as m-NpSB could form stable monolayer on pure water surface with novel phase transition process. The detailed changes of nanostructures were demonstrated around the phase transition region. Many methods have been used to characterize the ligand and the

corresponding complex films. A reasonable model was proposed to explain the novel phase transition process, as shown in **Figure 10**. When the ligand m-NpSB was spread on water surface, a smooth plain film was formed, which had also been verified by the AFM and XRD data. With the increment of surface pressure near the transition point, due to the spatial hindrance and lower energy level induced by the molecular rigidity and size, some molecules changed their conformational alignment and became more declined to surface, which could be well monitored by the AFM measurement at different surface pressures. After the point, the molecules completely aggregated to form fiber-like superstructure due to the high surface pressure and strong π–π stacking of aromatic moieties. Then, a change from two-dimensional (2D) to three-dimensional (3D) morphology was accomplished. The research work results provide distinct clues for the design and the fabrication of the aligned film structures at the air/water interface.

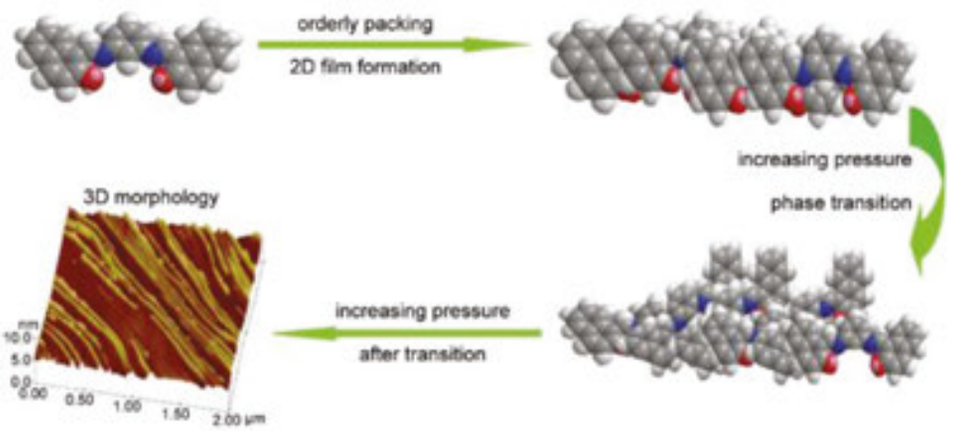


**Figure 10.** Schematic illustration of the phase behaviors of m-NpSB at air/water interface.

In addition, some achiral Cu(II)-coordinated Schiff base complexes containing aromatic structures were synthesized and their interfacial self-assemblies at the air/water interface were investigated [26]. The Schiff base complex molecules with naphthyl groups tended to form J-aggregate in the Langmuir-Blodgett (LB) films transferred from water surface. By investigation of atomic force microscopy shown in **Figure 11**, a multilayer film or three-dimensional structures were observed. It was interesting to note that the LB films of achiral compound Cu-NA with naphthyl segment and without methyl groups transferred from water surface showed chirality, which could be due to a cooperative stereoregular π–π stacking of the functional groups in a helical sense.

In another research work, a naphthyl-containing Schiff base derivative was synthesized, and its coordination with various metal ions at the air/water interface has been investigated [27]. Different nanostructures and interfacial coordination were obtained in the monolayers with metal ion subphase. And only the Cu(II)-coordinated composite film demonstrated supramolecular chirality. A possible organization mechanism at the air/water interface was suggested, as shown in **Figure 12**. When spreading on the subphase containing Cu(II) ion, an in situ coordination occurred between Cu(II) ion and the two hydrophilic groups. Due to this coordi-

http://dx.doi.org/10.5772/65122

nation and spatial hindrance, the long side of the triangle molecule would contact with the water surface, and the adjacent molecules are suggested to align cooperatively in a helical sense. Although both the left- and right-handed helical sense will occur due to the confinement of a two-dimensional platform, one kind of the helical sense could possibly be predominant, and thus we got a macroscopic chirality of the complex films.

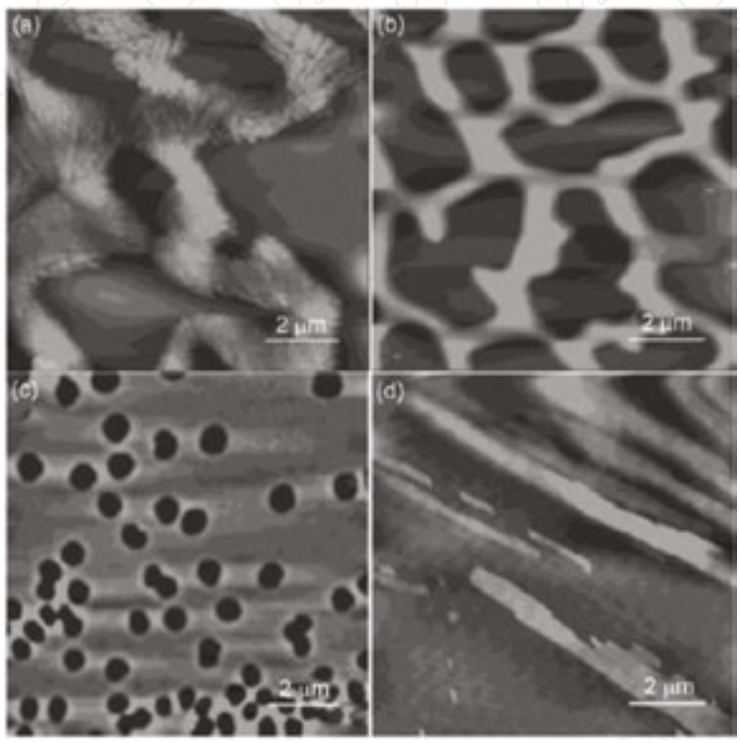


**Figure 11.** AFM images of one-layer LB films on pure water surface at surface pressure of 15 mN $m^{-1}$. (a) Cu-SA; (b) Cu-SAM; (c) Cu-NA; and (d) Cu-NAM.

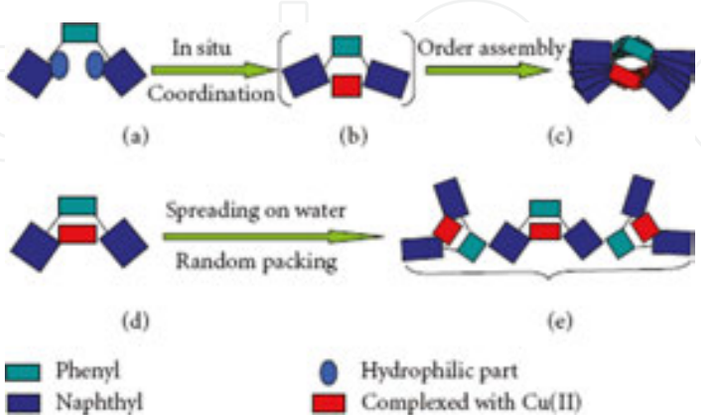


**Figure 12.** A possible schematic illustration on the formation of the chiral assemblies: (a) ligand molecule; (b) in situ Cu(II)-coordinated complex; (c) stacked in a helical sense to form chiral assembly; (d) preformed Cu(o-NpSB); (e) stacked in a random way.

## 3. Preparation and self-assembly of some functionalized supramolecular gels

In recent years, supramolecular gels have demonstrated more attentions due to the organized three-dimensional nanostructures and potential wide applications on functionalized drug delivery substrates and wastewater treatment [28–32]. The main driving forces in gel formations are cooperative noncovalent interactions, such as hydrogen bonding, π–π stacking, host-guest interaction, and so on [33–37]. The designed properties need the preparation of various functional gels with organized and controllable nanostructures [38–41]. In this section, we have showed some typical gel systems, including amide amphiphiles, binary gelators, graphene oxide composites, and AuNPs composites.

Firstly, two cholesterol amide derivatives with azobenzene substituent groups have been synthesized, and their gelation behaviors have also been investigated [42]. The experimental data revealed that the compound with headgroups of hydrogen units could only form gel in DMF, whereas the other compound with headgroups of methyl units cannot gelate any used solvent. Under UV light irradiation, the change of trans-cis isomerization in azobenzene segment appeared, which resulted in the gel-sol transition, as shown in **Figure 13**. In addition, the gel could be recovered by the reverse cis-trans isomerization process after visible light exposure. At the same time, the bulk solution with the macroscopic gel to sol transition became transparent.

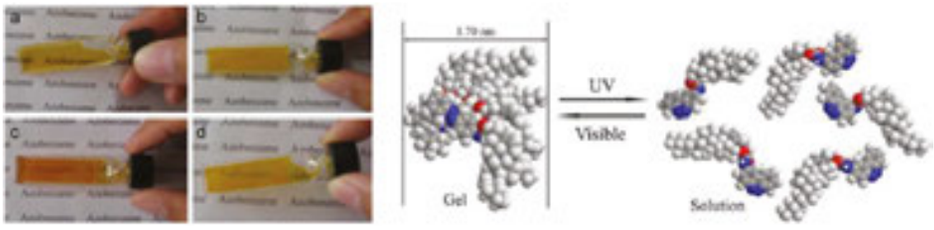


**Figure 13.** Left, Photographs of Ch-azo in hot DMF solution (a), formed gel in room temperature (b), after UV irradiation for 170 min (c), and subsequent visible irradiation for 40min (d). Right, Schematic representation of photo-induced gel-sol transition of DMF gel of Ch-azo.

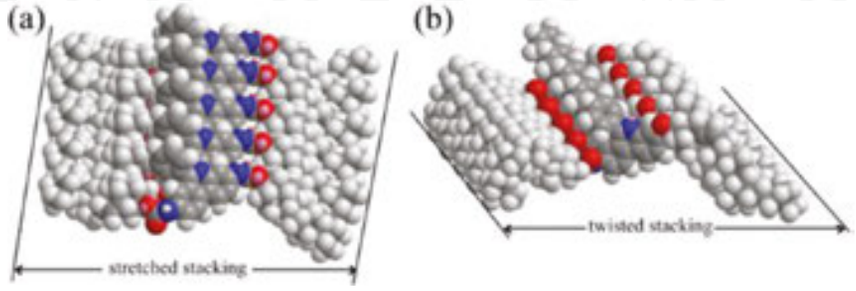


**Figure 14.** Rational assembly modes of CH-PY organogels in stretched stacking (a) and twisted stacking (b), respectively.

http://dx.doi.org/10.5772/65122

In addition, we have characterized the gelation behaviors of some bolaform cholesteryl amide compounds with large conjugated spacer [43, 44]. We found that the formed nanostructures and self-assembly process in organogels could be regulated by solvent change. Morphological characterization showed different aggregates, including wrinkle, belt, and fiber. We proposed possible self-assembly modes in gels, as shown in **Figure 14**. Different solvents could adjust molecular conformation to self-assemble and form twisted stretched stacking nanostructures.

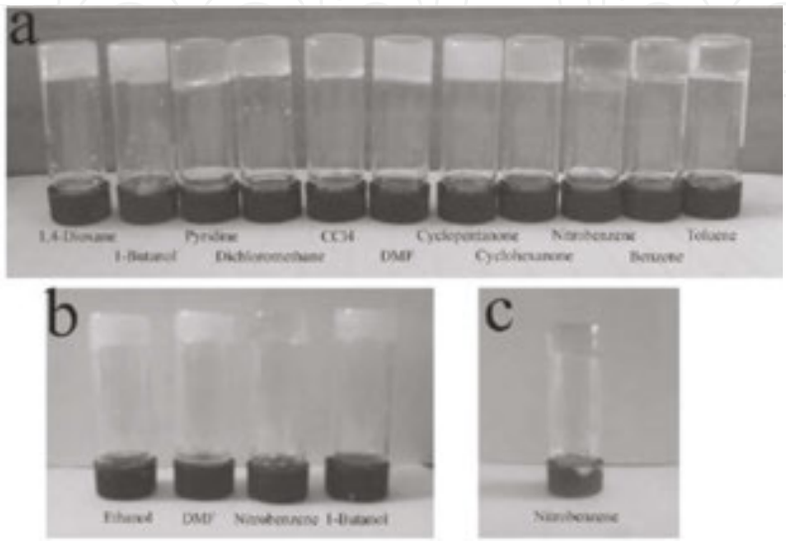


**Figure 15.** Photographs of organogels of GC16 (a), GC14 (b), and GC12 (c) in different solvents.

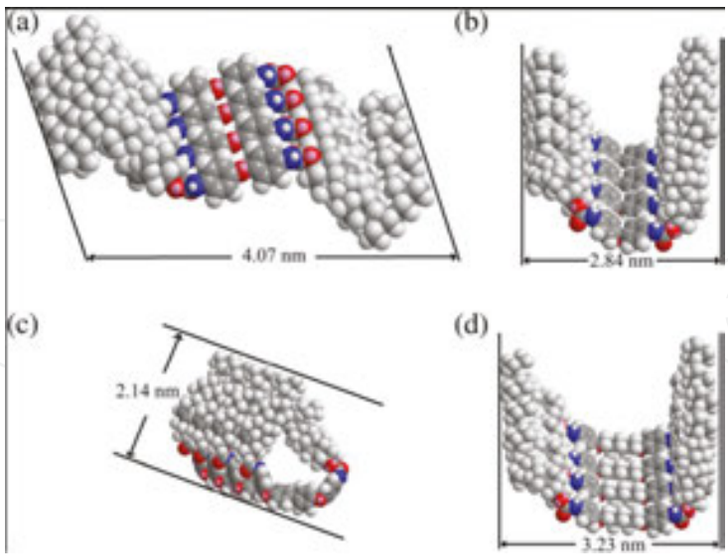


**Figure 16.** Rational assembly modes of CH-C1, CH-C3, and CH-C4 in gels. Experimental values of CH-C1 in 1,4-dioxane and nitrobenzene (a, b), CH-C3 in nitrobenzene (c), and CH-C4 in nitrobenzene (d).

In another work, we have demonstrated gelation behaviors of some glutamic acid diethyl ester amide compounds [45]. The obtained data indicated that the length of substituted alkyl chains

in gelator skeletons showed obvious regulation in gel formation. The photographs of all organogels in different solvents are shown in **Figure 15**. The reasonable explanation for the strong gelation behaviors for GC16 can be due to the enhanced hydrophobic force and organized spatial conformation.

Next, the gelation behaviors of some bolaform cholesteryl amide compounds with different kinds of spacers were demonstrated [46–50]. The obtained experimental results showed that these suitable flexible/rigid segments in spacers were helpful to form gels. Considering the all obtained data, some possible packing modes of these gelators were proposed and schematically shown in **Figure 16**. Due to the flexibility of spacers in the molecular skeleton and different intermolecular forces with solvents, after the intermolecular hydrogen bonding and orderly stacking in different solvents, various repeating units with different lengths were obtained.

In another research work, some binary organogels based on glutamic acid derivatives and acids with different molecular skeletons were designed and prepared [51]. The obtained results demonstrated that the suitable solvents or volume ratios in binary solvents were favorable for gel formation due to cooperative intermolecular interactions. In addition, the gelation behaviors in ethanol/water mixed solvents were also investigated, as shown in **Figure 17**. Interestingly, the results indicated the present mixtures can also form opaque organogels in mixed solvents with different volume ratios of mixed solvents. For example, GC2 can form gels in ethanol/water mixed solvents from the range of 2:1–1:5. The present experimental results suggested that some factors, such as solvents as well as the volume ratios of mixed solvents, aromatic/alkyl cores, and molecular skeletons in acid derivatives, could efficiently change and regulate the gelling abilities of these binary mixtures. Rational assembly modes in organogels were proposed and discussed.

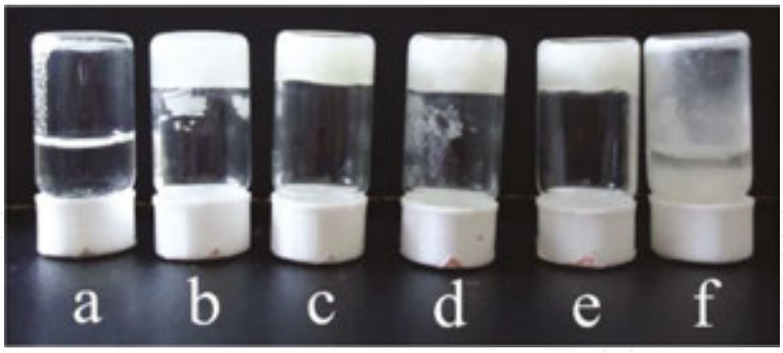


**Figure 17.** Photographs of GC2 organogels from ethanol/water mixed solvent with the volume ratios of 5:1, 2:1, 1:1, 1:2, 1:5, and 1:10 (a, b, c, d, e, and f, respectively).

In another continuous work, the gelation behaviors of binary organogels composed of azobenzene amino derivatives and fatty acids with different alkyl chains in various organic solvents were designed and investigated [52]. Their gelation behaviors in 20 solvents were tested as new binary organic gelators. Longer alkyl chains in molecular skeletons in present gelators are favorable for the gelation of organic solvents. Morphological studies revealed that the gelator molecules self-assemble into different aggregates from lamella, wrinkle, to belt with

http://dx.doi.org/10.5772/65122

change of solvents, as shown in **Figure 18**. In addition, it is interesting to note that these belt aggregates showed a tendency to aggregate together due to highly directional intermolecular interactions and/or solvent evaporation. The difference of morphologies can be mainly due to the different strengths of the intermolecular hydrophobic force between alkyl chains of fatty acids, which have played an important role in regulating the intermolecular orderly stacking and formation of special aggregates.

In another system, we have investigated the gelation behaviors of binary gelators, including glutamic acid amino derivative/azobenzene amino compounds and fatty acids [53, 54]. Considering the obtained XRD data, two possible assembly modes of Glu-C18 were proposed and schematically shown in **Figure 19**. For the Glu-C18 gels in some solvents, such as toluene, the layer distance in gel structures appeared at 3.2 nm due to the penetration of alkyl chains of the neighboring gel molecules. In another kind of gel, repeating unit with 2 nm length was obtained because of parallel chains.

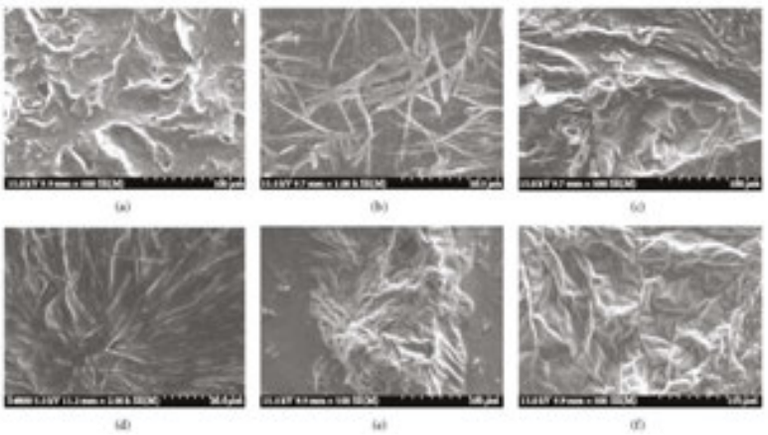

**Figure 18.** SEM images of xerogels: (a and c–f): C18-Azo, C16-Azo, C14-Azo, C18-Azo-Me, and C16-Azo-Me in ethanolamine, respectively; (b) C16-Azo in nitrobenzene.

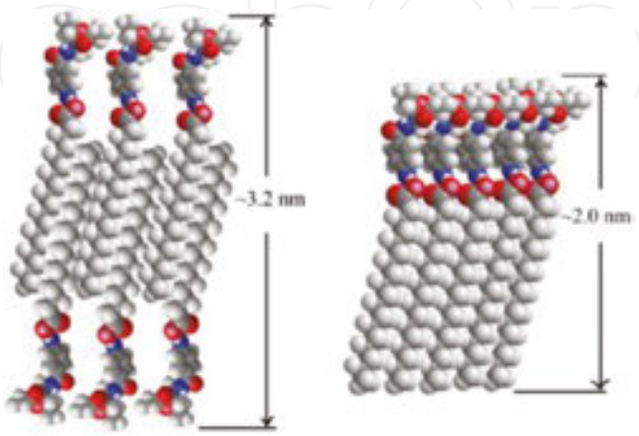


**Figure 19.** Two possible assembly modes for Glu-C18 organogels in different solvents.

In recent years, graphene oxide (GO)-based nanomaterials have drawn abundant attentions. In recent report, we have prepared organogels through cationic gemini compounds-GO composites [55]. The obtained data demonstrated that the gelation behaviors could be regulated by change of substituted headgroups in compounds. In addition, different self-assembly nanostructures were obtained, as shown in **Figure 20**, indicating special assembly modes in gels. Moreover, it is well known that the thickness of GO sheet (about 0.5–1.0 nm) is larger than the theoretical value of graphene layer (0.34 nm). This is mainly due to the abundant oxygen-containing groups (hydroxyl and epoxy groups) remaining on the surface of the GO sheets. A possible mechanism for headgroup effects on self-assembly and as-prepared nanostructures is proposed.

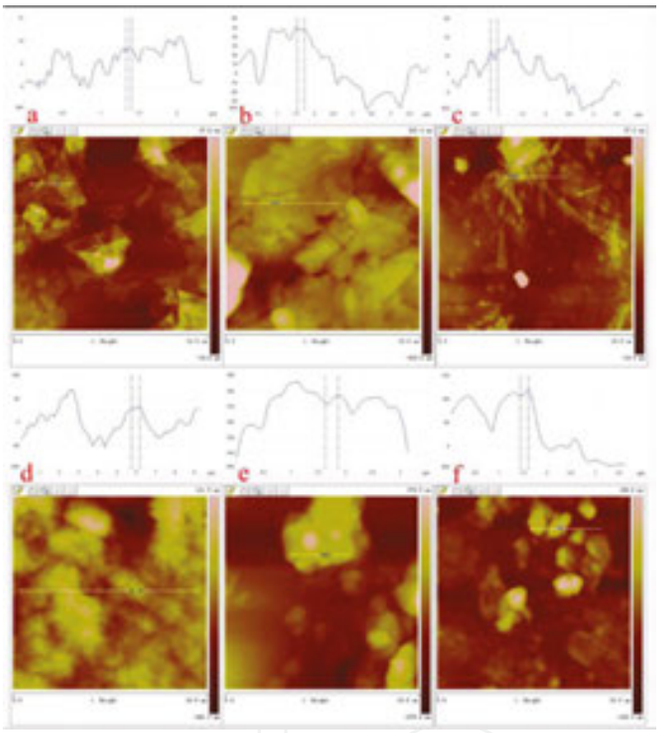


**Figure 20.** AFM images with section analysis of xerogels. C16Py-GO gels, BPy-GO gels, and CTAB-GO gels in DMF (a, b, and c) and in THF (d, e, and f).

In another continuous work, we have reported the preparation of composite supramolecular organogels by self-assembling cationic functional gemini compound-GO nanocomposites [56]. The gel formation properties of as-prepared nanocomposites present in different organic solvents could be controlled by regulating symmetry in skeletons of amphiphilic compounds. In combination with the spectral and morphological data of as-prepared organogels, some possible and reasonable self-assembly modes for present gemini compound-GO nanocomposite gels are given and demonstrated in **Figure 21**. As for C18-6-0/GO composite and C18-6-6/GO gel with shorter substituent alkyl chain in gemini molecules, due to the intermolecular weak van der Waals interaction of substituent alkyl chains caused by asymmetric molecular skeletons, disorderly stacking appeared in the interlayer of self-assembled nanocomposite

http://dx.doi.org/10.5772/65122

units, which seemed to be difficult to connect each other as fundamental building blocks to fabricate three-dimensional organized net to form gel state. So C18-6-6/GO composite can only fabricate one kind of gel in present 20 organic solvents. With the increment of alkyl chain to carbon 12 and 18, for the case of C18-6-12/GO and C18-6-18/GO composites, longer alkyl chains in molecular skeletons helped to increase hydrophobic force and flexibility in self-assembly process. After integration with GO, organized stacking units appeared in various solvents with the strong van der Waals force of gemini compounds with functional oxygen-containing chemical groups on surface or at edge.

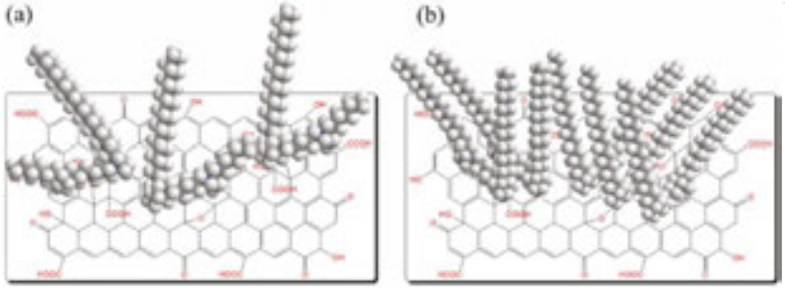


**Figure 21.** Schematic pictures of different assembly modes in C18-6-6/GO gels with asymmetric skeleton (a) and C18-6-18/GO gels with symmetric skeleton (b).

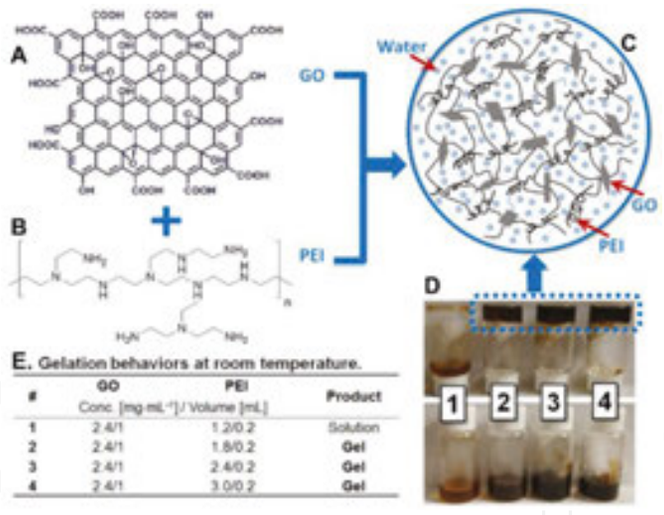


E. Gelation behaviors at room temperature.

| # | GO Conc. [mg·mL⁻¹] / Volume [mL] | PEI Conc. [mg·mL⁻¹] / Volume [mL] | Product |
|---|---|---|---|
| 1 | 2.4/1 | 1.2/0.2 | Solution |
| 2 | 2.4/1 | 1.8/0.2 | Gel |
| 3 | 2.4/1 | 2.4/0.2 | Gel |
| 4 | 2.4/1 | 3.0/0.2 | Gel |

**Figure 22.** Schematic depiction of the formation of GO/PEI gels. (A) GO and (B) amine-rich PEI was combined to give (C) GO/PEI hydrogels. (D and E) Gelation pictures.

In another work, the preparation of GO/polyethylenimine (PEI) and GO/chitosan (CS) hydrogels as dye adsorbents for wastewater treatment was reported [57, 58]. The GO/PEI hydrogels were obtained through both hydrogen bonding and electrostatic interactions between amine-rich PEI and GO sheets. **Figure 22** depicts the complete preparation process of GO/PEI hydrogels by combining the GO suspension and the PEI aqueous solution. The as-prepared GO/PEI hydrogels exhibited good removal rates for both MB and RhB in accordance with the pseudo-

second-order model. More importantly, the dye-adsorbed hydrogels can be conveniently separated from an aqueous environment, suggesting potential large-scale applications of the GO-based hydrogels for organic dye removal and wastewater treatment.

In a recent report, some composite hydrogels through GO and multiamine molecules have been designed and prepared from the self-assembly of GO in the presence of multiamine molecules, including diethylenetriamine (DETA) and triethylenetetramine (TETA) [59]. The micro/nanostructures in nanocomposite hydrogel were characterized by morphological investigation. The characteristic bands of graphene samples in Raman spectra appeared, as shown in **Figure 23**. This change can be mainly attributed to the self-assembly of GO in the net-like composite nanostructures. The next adsorption properties demonstrate that these designed and synthesized GO-based composite hydrogels can act as efficient absorbents for dye removal from wastewater in well accordance with the pseudo-second order model.

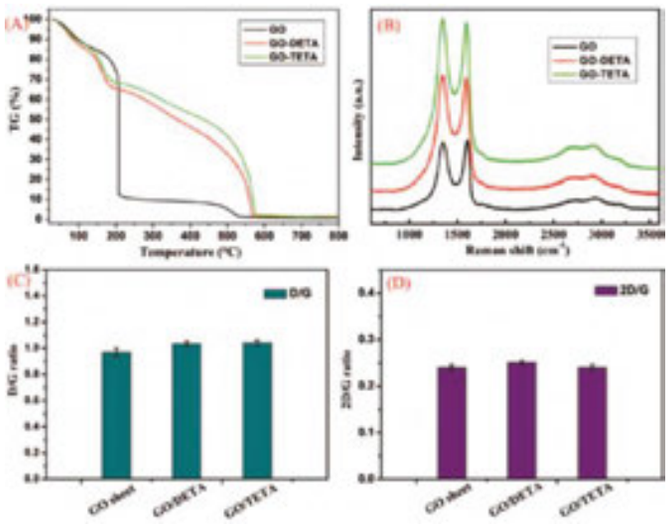


**Figure 23.** TG curves (A) and Raman spectra (B) of lyophilized GO sheet, GO-DETA hydrogel, and GO-TETA hydrogel at concentration of 0.25 wt%, respectively. (C) and (D) are D/G and 2D/G ratios of the Raman spectra shown in B, respectively.

In addition, we have reported the synthesis of RGO/PEI/Ag and RGO/CS/Ag composite gel materials and evaluated its dye degradation capacity [60, 61]. The CS molecule was chosen for its functional amine segments in the molecular skeleton that can form porous gel nanostructures through interactions such as hydrogen bonding. The photographs of the GO aqueous solution, GO/CS gel, RGO/CS gel, and RGO/CS/Ag composite gels are demonstrated in **Figure 24**. The formed composite gels can provide enough space among its 3D nanostructure for the adsorption and degradation of organic dyes. In addition, the in situ formed silver nanoparticles were homogeneously anchored on RGO surface to form a ternary nanocomposite material. The data of photocatalytic capacity experiments suggest that the prepared 3D GO-based hydrogels can efficiently remove dyes and exhibit good photocatalytic performance for presently used RhB and MB single or mixed solutions in accordance with the pseudo-second order model.

http://dx.doi.org/10.5772/65122

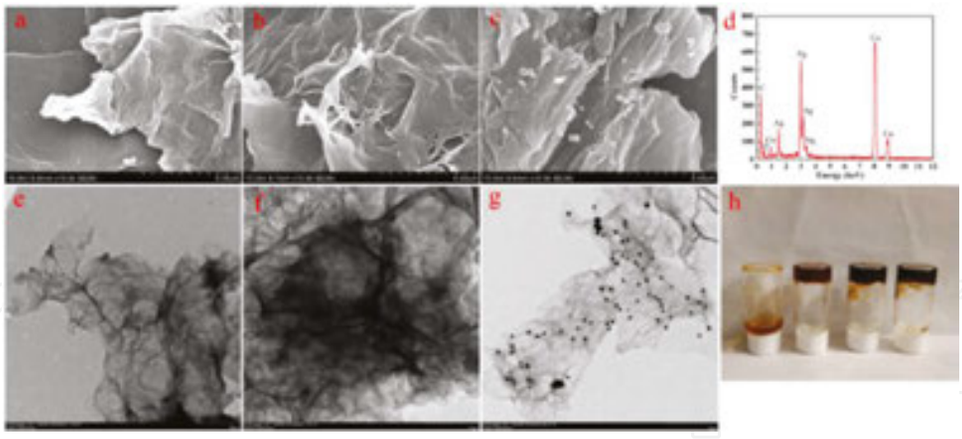


**Figure 24.** SEM and TEM images for the lyophilized GO/CS hydrogel (a, e), RGO/CS hydrogel (b, f), and RGO/CS/Ag hydrogel (c, g). (d) EDXS taken on the RGO/CS/Ag hydrogel shown in part (g). (h) Photographs of the following: GO aqueous solution, GO/CS, RGO/CS, and RGO/CS/Ag composite hydrogels (from left to right).

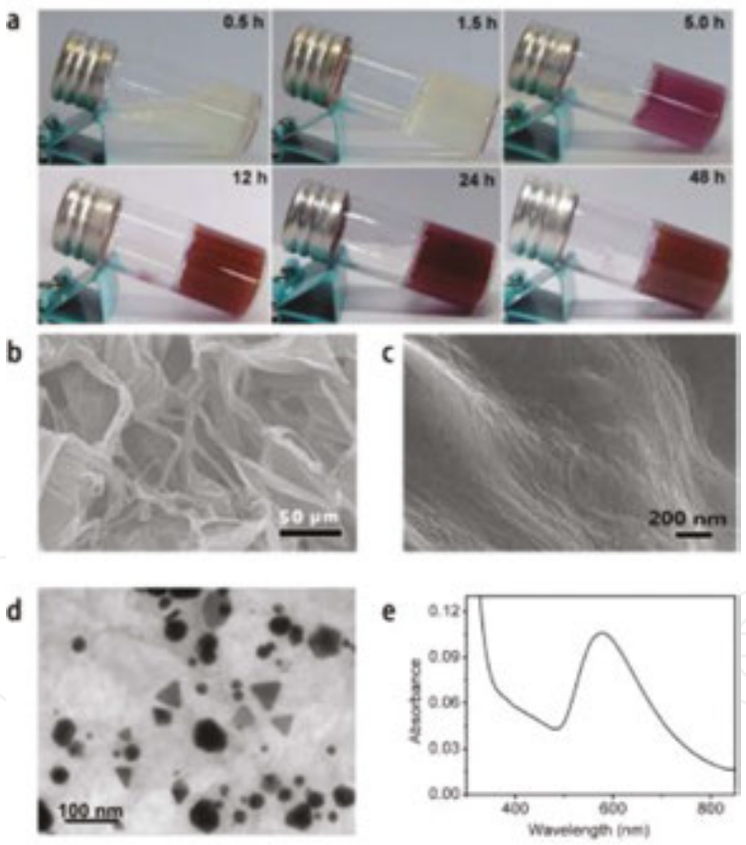


**Figure 25.** Photographs and morphological characterization of the obtained collagen-AuNPs composite hydrogel: (a) photographs of the formation and color change of the collagen hydrogel versus time when a collagen aqueous acidic solution was mixed with an aliquot of HAuCl4 solution under ambient conditions; (b) and (c) SEM images at low and high magnification of a typical collagen-based hydrogel; (d) TEM image of the AuNP spreading throughout the hydrogel network; (e) UV–vis absorption spectrum of the collagen-based hydrogel containing AuNPs, showing the characteristic SPR absorbance.

In a recent work, in order to enhance the mechanical behaviors of hydrogels, we have designed and prepared an injectable and self-healing collagen-protein-based hydrogel by a gold-biomineralization-triggered self-assembly [62]. The locally synthesized gold nanoparticles are demonstrated to tune the mechanical properties of the collagen-based hydrogels, in which reversible weak interactions between collagen chains and gold nanoparticles endow the hydrogels with shear-thinning and self-healing functions. The photographs and morphological characterization were shown in **Figure 25**. Such biocompatible collagen-based hydrogels have been developed as a novel tool for localized delivery and sustained release of therapeutic drugs, with the advantages to reduce the drug dosage, to lower the toxicity, and to improve the bioavailability.

## 4. Conclusion and perspective

We are working on the design, preparation, and self-assembly of functionalized LB films and supramolecular gels. In this chapter, various kinds of LB films including bolaform amphiphiles, gemini-type compounds, inorganic-organic hybrid composites, and supramolecular gels through functionalized amide amphiphiles/binary gelators/graphene oxide nanocomposites have all been demonstrated and investigated. The above research work may give the potential perspective for the design and preparation of new self-assembly systems and nanomaterials. In closing, LB films and supramolecular gels can be regarded as good research platforms for various assembly systems. In addition, supramolecular self-assembly demonstrate charming applications, such as physics, biosensors, catalysis, nanomaterials, environmental treatment, and so on. It can be expected that future research systems of LB films and supramolecular gels will be relative to the novel applications and special nanostructures to obtain new functional nanocomposites and nanostructures. The development of preparation of functionalized nanomaterials with self-assembled nanostructures has been fascinating in future.

## Acknowledgements

The authors like to extend their thanks to the National Natural Science Foundation of China (Project No. 21473153), the Support Program for the Top Young Talents of Hebei Province, the China Postdoctoral Science Foundation (No. 2015M580214), the Science Foundation for the Excellent Youth Scholars from Universities and Colleges of Hebei Province (No. YQ2013026), the Post-graduate's Innovation Fund Project of Hebei Province (No. 2016SJBS009), the Scientific and Technological Research and Development Program of Qinhuangdao City (No. 201502A006), and the Open Funding Project of the National Key Laboratory of Biochemical Engineering (No. 2013KF-02).

## Author details

Tifeng Jiao[1,2*], Ruirui Xing[1,2], Kai Ma[1] and Lexin Zhang[1]

*Address all correspondence to: tfjiao@ysu.edu.cn

1 Hebei Key Laboratory of Applied Chemistry, School of Environmental and Chemical Engineering, Yanshan University, Qinhuangdao, P. R. China

2 National Key Laboratory of Biochemical Engineering, Institute of Process Engineering, Chinese Academy of Sciences, Beijing, P. R. China

## References

[1] De Barros A, Constantino CJL, Bortoleto JRR, Da Cruz NC, Ferreira M. Incorporation of gold nanoparticles into Langmuir-Blodgett films of polyaniline and montmorillonite for enhanced detection of metallic ions. Sensor Actuat B-Chem 2016;236:408–417.

[2] Debnath P, Chakraborty S, Deb S, Nath J, Dey B, Bhattacharjee D, Hussain SA. Stability of J-aggregated species in an indocarbocyanine dye in Langmuir–Blodgett films. J Lumin 2016;179:287–296.

[3] Grauby-Heywang C, Moroté F, Mathelié-Guinlet M, Gammoudi I, Faye NR, Cohen-Bouhacina T. Influence of oxidized lipids on palmitoyl-oleoyl-phosphatidylcholine organization, contribution of Langmuir monolayers and Langmuir–Blodgett films. Chem Phys Lipids 2016;200:74–82.

[4] Wang L, Li Y, Wang Q, Zou L, Ye B. The construction of well-aligned MWCNTs-PANI Langmuir–Blodgett film modified glassy carbon electrode and its analytical application. Sensor Actuat B-Chem 2016;228:214–220.

[5] Wang KH, Wu JY, Chen LH, Lee YL. Architecture effects of glucose oxidase/Au nanoparticle composite Langmuir-Blodgett films on glucose sensing performance. Appl Surf Sci 2016;366:202–209.

[6] Saha S, Ghosh M, Dutta B, Chowdhury J. Silver coated gold nanocolloids entrapped in organized Langmuir–Blodgett film of stearic acid: Potential evidence of a new SERS active substrate. Appl Surf Sci 2016;362:364–373.

[7] Harish TS, Viswanath P. Annealing assisted structural and surface morphological changes in Langmuir–Blodgett films of nickel octabutoxy phthalocyanine. Thin Solid Films 2016;598:170–176.

[8] Wang F, Chi C, Yu B, Ye B. Simultaneous voltammetric determination of dopamine and uric acid based on Langmuir–Blodgett film of calixarene modified glassy carbon electrode. Sensor Actuat B-Chem 2015;221:1586–1593.

[9] de Araújo FT, Caseli L. Rhodanese incorporated in Langmuir and Langmuir–Blodgett films of dimyristoylphosphatidic acid: Physical chemical properties and improvement of the enzyme activity. Colloids Surf B Biointerfaces 2016;141:59–64.

[10] Miura YF, Matsui H, Inoue K, Hoshino J, Ikegami K. Structure and properties of the highly conductive Langmuir–Blodgett films based on ditetradecyldimethylammonium-Au(dmit)$_2$ salt. Synthetic Met 2015;207:54–64.

[11] Pandit P, Banerjee M, Pandey KK, Sharma SM, Gupta A. Role of substrate in melting behavior of Langmuir–Blodgett films. Colloids Surface A 2015;471:159–163.

[12] Pazinato J, Hoffmeister DM, Naidek KP, Westphal E, Gallardo H, Winnischofer H. Amphiphilic ruthenium bipyridine complex containing long-chain azopyridine group and the mechanism of electron transfer in Langmuir-Blodgett films. Electrochim Acta 2015;153:574–582.

[13] Zou L, Li Y, Cao S, Ye B. A new voltammetric sensor for sensitive and selective determination of xanthine based on DNA and polyaniline composite Langmuir–Blodgett film. Talanta 2014;129:346–351.

[14] Ferreira GC, Caseli L, Péres LO. Block copolymers of o-PPV organized at the molecular scale as Langmuir and Langmuir–Blodgett films. Synthetic Met 2014;194:65–70.

[15] Karthik C, Manjuladevi V, Gupta RK, Kumar S. Pattern formation in Langmuir–Blodgett films of tricycloquinazoline based discotic liquid crystal molecules. J Mol Struct 2014;1070:52–57.

[16] Jiao T, Liu M. Supramolecular assemblies and molecular recognition of amphiphilic Schiff bases with barbituric acid in organized molecular films. J Phys Chem B 2005;109(7):2532–2539.

[17] Jiao T, Liu M. Supramolecular assemblies of a new series of gemini-type Schiff base amphiphiles at the air/water interface: interfacial nanoarchitectures, in situ coordination and spacer effect. Langmuir 2006;22(11):5005–5012.

[18] Jiao T, Cheng C, Xi F, Liu M. Metal ion modulated organization and nanostructure construction of amphiphilic tyrosine-based bolaamphiphile at the air/water interface. Thin Solid Films 2006;503(1-2):230–235.

[19] Cheng C, Jiao T, Tang R, Chen E, Liu M, Xi F. Compression-induced hierarchical nanostructures of a poly(ethylene oxide)-block-dendronized polymethacrylate copolymer at the air/water interface. Macromolecules 2006;39(19):6327–6330.

[20] Guo Z, Jiao T, Liu M. Effect of substituent position in coumarin derivatives on the interfacial assembly: reversible photodimerization and supramolecular chirality. Langmuir 2007;23(4):1824–1829.

[21] Zhong L, Jiao T, Liu M. Synthesis and assembly of gold nanoparticles in organized molecular films of gemini amphiphiles. Langmuir 2008;24(20):11677–11683.

[22] Jiao T, Leca-Bouvier BD, Boullanger P, Blum LJ, Girard-Egrot AP. Phase behavior and optical investigation of two synthetic luminol derivatives and glycolipid mixed monolayers at the air-water interface. Colloid Surf A 2008;321(1-3):137–142.

[23] Jiao T, Leca-Bouvier BD, Boullanger P, Blum LJ, Girard-Egrot AP. A chemiluminescent Langmuir–Blodgett membrane as the sensing layer for the reagentless monitoring of an immobilized enzyme activity. Colloids Surf A 2010;354(1-3):284–290.

[24] Jiao T, Li X, Zhang Q, Duan P, Zhang L, Liu M, Luo X, Li Q, Gao F. Interfacial assembly of a series of trigonal Schiff base amphiphiles in organized molecular films. Colloids Surf A 2012;407(5):108–115.

[25] Jiao T, Liu M. Phase behaviors and 2D-3D morphological transition of aromatic Schiff base derivatives in organized molecular films. Acta Phys-Chim Sin 2012;28(6):1418–1424.

[26] Jiao T, Li X, Zhang Q, Li Q, Zhou J, Gao F. Interfacial assembly of a series of Cu(II)-coordinated Schiff bases complexes: orderly nanostructures and supramolecular chirality. Sci China Technol Sci 2013;56(1):20–24.

[27] Jiao T, Xing R, Zhang Q, Lv Y, Zhou J, Gao F. Self-assembly, interfacial nanostructure, and supramolecular chirality of the Langmuir-Blodgett films of some Schiff base derivatives without alkyl chain. J Nanomater 2013;2013:297564.

[28] Kowalczuk J, Rachocki A, Bielejewski M, Tritt-Goc J. Effect of gel matrix confinement on the solvent dynamics in supramolecular gels. J Colloid Interf Sci 2016;472:60–68.

[29] Marcos X, Pérez-Casas S, Llovo J, Concheiro A, Alvarez-Lorenzo C. Poloxamer-hydroxyethyl cellulose-$\alpha$-cyclodextrin supramolecular gels for sustained release of griseofulvin. Int J Pharm 2016;500(1-2):11–19.

[30] Zeng X, Sun Z, Wang H, Wang Q, Yang Y. Supramolecular gel composites reinforced by using halloysite nanotubes loading with in-situ formed $Fe_3O_4$ nanoparticles and used for dye adsorption. Compos Sci Technol 2016;122:149–154.

[31] Tanaka T, Gotanda R, Tsutsui A, Sasayama S, Yamamoto K, Kimura Y, Kadokawa J. Synthesis and gel formation of hyperbranched supramolecular polymer by vine-twining polymerization using branched primer–guest conjugate. Polymer 2015;73:9–16.

[32] Chu X, Xing P, Li S, Ma M, Hao A. Inorganic salt-tuned multiple self-assemblies of supramolecular β-cyclodextrin gel. Colloid Surface A 2014;461:11–17.

[33] Zhu F, Lin XY, Wu ZL, Cheng L, Yin J, Song Y, Qian J, Zheng Q. Processing tough supramolecular hydrogels with tunable strength of polyion complex. Polymer 2016;95:9–17.

[34] Simões SMN, Veiga F, Ribeiro ACF, Figueiras AR, Taboada P, Concheiro A, Alvarez-Lorenzo C. Supramolecular gels of poly-$\alpha$-cyclodextrin and PEO-based copolymers for controlled drug release. Eur J Pharm Biopharm 2014;87(3):579–588.

[35] Cheng X, Jin Y, Sun T, Qi R, Li H, Fan W. An injectable, dual pH and oxidation-responsive supramolecular hydrogel for controlled dual drug delivery. Colloids Surf B 2016;141:44–52.

[36] Klaewklod A, Tantishaiyakul V, Hirun N, Sangfai T, Li L. Characterization of supramolecular gels based on β-cyclodextrin and polyethyleneglycol and their potential use for topical drug delivery. Mater Sci Eng-C 2015;50:242–250.

[37] Lin Y, Li L, Li G. A new supramolecular gel via host–guest complexation with cucurbit[8]uril and N-(4-diethylaminobenzyl)chitosan. Carbohydr Polym 2013;92(1):429–434.

[38] Yang Y, Chen X, Huang D, Ye W. Supramolecular gel based on the cyclodextrin inclusion assembly of Ag-$Fe_3O_4$ nanodimers and Pluronic F127. Colloids Surf A 2013;436:467–473.

[39] Delbecq F. Supramolecular gels from lipopeptide gelators: Template improvement and strategies for the in-situ preparation of inorganic nanomaterials and for the dispersion of carbon nanomaterials. Adv Colloid Interface Sci 2014;209:98–108.

[40] Zhang YM, Zhang WQ, Li JQ, Dang JP, Wei TB. Cadmium-induced supramolecular hydrogels: Reversible sol–gel transitions induced by EDTA and acid/base exchange. Mater Lett 2012;82:227–229.

[41] Jin H, Dai XH, Wu C, Pan JM, Wang XH, Yan YS, Liu DM, Sun L. Rational design of shear-thinning supramolecular hydrogels with porphyrin for controlled chemotherapeutics release and photodynamic therapy. Eur Polym J 2015;66:149–159.

[42] Jiao T, Wang Y, Gao FQ, Zhou J, Gao FM. Photoresponsive organogel and organized nanostructures of cholesterol imide derivatives with azobenzene substituent groups. Prog Nat Sci: Mater Int 2012;22(1):64–70.

[43] Jiao T, Gao FQ, Wang Y, Zhou J, Gao FM, Luo X. Supramolecular gel and nanostructures of bolaform and trigonal cholesteryl derivatives with different aromatic spacers. Curr Nanosci 2012;8(1):111–116.

[44] Jiao TF, Gao FQ, Shen XH, Zhang QR, Zhang XF, Zhou JX, Gao FM. Self-assembly and nanostructures in organogels based on a bolaform cholesteryl imide compound with conjugated aromatic spacer. Materials 2013;6(12):5893–5906.

[45] Jiao T, Wang R, Zhang Q, Yan X, Zhou J, Gao F. Nanostructures and substituent alkyl chains effect on assembly of organogels based on some glutamic acid diethyl ester imide derivatives. Curr Nanosci 2013;9(4):536–542.

[46] Jiao T, Gao F, Zhang Q, Zhou J, Gao F. Spacer effect on nanostructures and self-assembly in organogels via some bolaform cholesteryl imide derivatives with different spacers. Nanoscale Res Lett 2013;8:406.

[47] Jiao T, Huang Q, Zhang Q, Xiao D, Zhou J, Gao F. Self-assembly of organogels via new luminol imide derivatives: diverse nanostructures and substituent chain effect. Nanoscale Res Lett 2013;8:278.

[48] Jiao T, Wang Y, Zhang Q, Zhou J, Gao F. Regulation of substituent groups on morphologies and self-assembly of organogels based on some azobenzene imide derivatives. Nanoscale Res Lett 2013;8:160.

[49] Jiao T, Ma K, Shen X, Zhang Q, Li X, Zhou J, Gao F. Self-assembly and soft material preparation of binary organogels via aminobenzimidazole/benzothiazole and acids with different alkyl substituent chains. J Nanomater 2013;2013:762732.

[50] Shen X, Jiao T, Zhang Q, Guo H, Lv Y, Zhou J, Gao F. Nanostructures and self-assembly of organogels via benzimidazole/benzothiazole imide derivatives with different alkyl substituent chains. J Nanomater 2013;2013:409087.

[51] Guo H, Jiao T, Shen X, Zhang Q, Li A, Zhou J, Gao F. Binary organogels based on glutamic acid derivatives and different acids: solvent effect and molecular skeletons on self-assembly and nanostructures. Colloids Surf A 2014;447:88–96.

[52] Guo H, Jiao T, Shen X, Zhang Q, Li A, Gao F. Preparation and characterization of binary organogels via some azobenzene amino derivatives and different fatty acids: self-assembly and nanostructures. J Spectrosc 2014;2014:758765.

[53] Jiao T, Xing R, Shen X, Zhang Q, Zhou J, Gao F. Investigation of orderly nanostructures and assembly modes of binary organogels via glutamic acid amino derivative and different fatty acids. Integr Ferroelect: Int J 2014;151(1):31–41.

[54] Hu Y, Li Q, Hong W, Jiao T, Xing G, Jiang Q. Characterization of binary organogels based on some azobenzene compounds and alkyloxybenzoic acids with different chain lengths. J Spectrosc 2014;2014:970827.

[55] Jiao T, Wang Y, Zhang Q, Yan X, Zhao X, Zhou J, Gao F. Self-assembly and headgroup effect in nanostructured organogels via cationic amphiphile-graphene oxide composites. PLoS One 2014;9(7):e101620.

[56] Jiao T, Wang Y, Zhang Q, Yan X, Zhao X, Huo Q, Zhou J, Gao F. Organogels via gemini amphiphile-graphene oxide composites: self-assembly and symmetry effect. Sci Adv Mater 2015;7(9):1677–1685.

[57] Guo H, Jiao T, Zhang Q, Guo W, Peng Q, Yan X. Preparation of graphene oxide-based hydrogels as efficient dye adsorbents for wastewater treatment. Nanoscale Res Lett 2015;10:272.

[58] Zhao H, Jiao T, Zhang L, Zhou J, Zhang Q, Peng Q, Yan X. Preparation and adsorption capacity evaluation of graphene oxide-chitosan composite hydrogels. Sci China Mater 2015;58(10):811–818.

[59] Zhu K, Jiao T, Zhang L, Xing R, Guo R, Zhou J, Hou C, Zhang Q, Peng Q, Li X. Preparation and absorption capacity evaluation of composite hydrogels via graphene oxide and multi-amine molecules. Sci Adv Mater 2016;8(7):in press.

[60] Jiao T, Guo H, Zhang Q, Peng Q, Tang Y, Yan X, Li B. Reduced graphene oxide-based silver nanoparticle-containing composite hydrogel as highly efficient dye catalysts for wastewater treatment. Sci Rep-UK 2015;5:11873.

[61] Jiao T, Zhao H, Zhou J, Zhang Q, Luo X, Hu J, Peng Q, Yan X. Self-assembly reduced graphene oxide nanosheet hydrogel fabrication by anchorage of chitosan/silver and its potential efficient application toward dyes degradation for wastewater treatments. ACS Sustain Chem Eng 2015;3(12):3130–3139.

[62] Xing R, Liu K, Jiao T, Zhang N, Ma K, Zhang R, Zou Q, Ma G, Yan X. An injectable self-assembling collagen-gold hybrid hydrogel for combinatorial antitumor photothermal/photodynamic therapy. Adv Mater 2016;28(19):3669–3676.